Cluster Size Selectivity in the Product Distribution of Ethene Dehydrogenation on Niobium Clusters

J. Mark Parnis,*,†,‡ Eric Escobar-Cabrera,† Matthew G. K. Thompson,†,‡ J. Paul Jacula,†,‡ Rick D. Lafleur,†,‡ Alfredo Guevara-García,§ Ana Martínez,§,|| and David M. Rayner⊥

Department of Chemistry, Trent University, Peterborough, Ontario, Canada K9J 7B8, Department of Chemistry, Queen's University, Kingston, Ontario, Canada K7L 3N6, Instituto de Investigaciones en Materiales, UNAM, Circuito Exterior s/n Ciudad Universitaria, 04510, Coyoacán, México D.F., and Steacie Institute for Molecular Sciences, National Research Council of Canada, 100 Sussex Drive, Ottawa, Ontario, Canada K1A 0R6

Received: February 8, 2005; In Final Form: May 13, 2005

Ethene reactions with niobium atoms and clusters containing up to 25 constituent atoms have been studied in a fast-flow metal cluster reactor. The clusters react with ethene at about the gas-kinetic collision rate, indicating a barrierless association process as the cluster removal step. Exceptions are Nb_8 and Nb_{10}, for which a significantly diminished rate is observed, reflecting some cluster size selectivity. Analysis of the experimental primary product masses indicates dehydrogenation of ethene for all clusters save Nb_{10}, yielding either $Nb_nC_2H_2$ or Nb_nC_2. Over the range $Nb-Nb_6$, the extent of dehydrogenation increases with cluster size, then decreases for larger clusters. For many clusters, secondary and tertiary product masses are also observed, showing varying degrees of dehydrogenation corresponding to net addition of C_2H_4, C_2H_2, or C_2. With Nb atoms and several small clusters, formal addition of at least six ethene molecules is observed, suggesting a polymerization process may be active. Kinetic analysis of the Nb atom and several Nb_n cluster reactions with ethene shows that the process is consistent with sequential addition of ethene units at rates corresponding approximately to the gas-kinetic collision frequency for several consecutive reacting ethene molecules. Some variation in the rate of ethene pick up is found, which likely reflects small energy barriers or steric constraints associated with individual mechanistic steps. Density functional calculations of structures of Nb clusters up to Nb_6, and the reaction products $Nb_nC_2H_2$ and Nb_nC_2 ($n = 1...6$) are presented. Investigation of the thermochemistry for the dehydrogenation of ethene to form molecular hydrogen, for the Nb atom and clusters up to Nb_6, demonstrates that the exergonicity of the formation of Nb_nC_2 species increases with cluster size over this range, which supports the proposal that the extent of dehydrogenation is determined primarily by thermodynamic constraints. Analysis of the structural variations present in the cluster species studied shows an increase in C−H bond lengths with cluster size that closely correlates with the increased thermodynamic drive to full dehydrogenation. This correlation strongly suggests that all steps in the reaction are barrierless, and that weakening of the C−H bonds is directly reflected in the thermodynamics of the overall dehydrogenation process. It is also demonstrated that reaction exergonicity in the initial partial dehydrogenation step must be carried through as excess internal energy into the second dehydrogenation step.

Introduction

Research into the chemistry of transition metal clusters remains an intriguing area, due to the allure of cluster size-specific properties, which may sometimes be correlated with particular physical, structural or chemical properties of individual clusters. Aspects of this chemistry have been reviewed by Knickelbein,[1] showing that transition metal clusters are amenable to detailed theoretical and experimental investigation, often revealing provocative relationships between physical properties and chemical reactivity. In this paper, the interaction of neutral Nb clusters with ethene in a fast flow gas-phase reactor is reported. A particular impetus for the present work is the understanding of underlying cluster size-dependent factors that control the extent of dehydrogenation in the observed products.

* Corresponding author. E-mail: mparnis@trentu.ca.
† Trent University
‡ Queen's University.
§ UNAM. Circuito Exterior s/n Ciudad Universitaria.
|| E-mail: martina@matilda.iimatercu.unam.mx.
⊥ National Research Council of Canada.

As a result of its high reactivity and single, naturally occurring isotope, clusters of niobium figure particularly prominently in the development of metal cluster chemistry, and there have been several theoretical[2−6] and experimental studies[7−18] focused on Nb clusters. Early work by Morse et al.[11] showed that Nb clusters exhibit significant cluster-size selectivity, with particularly low reactivity noted for Nb_8, Nb_{10}, and Nb_{16} with D_2 and N_2. This result has been confirmed more recently by absolute rate coefficient measurement by Berces et al.[14] Zakin et al.[12] showed that these cluster masses, and Nb_{12}, showed low reactivity as cationic, neutral or anionic clusters with D_2. Later ICR work by Elkind et al.[10] confirmed these conclusions. Note that all such examples of cluster size selectivity in cluster reactivity rate are in contrast with the observed behavior of Nb clusters with CO[11] and isobutane,[13] for which only gradual increases in reaction rate coefficient with cluster size are observed.

Several groups have studied the dehydrogenation reactions of Nb clusters and cluster cations with benzene[15−18] and other alkenes.[8] The general tendency is toward highest degree of dehydrogenation in the mass range corresponding to clusters

10.1021/jp0506944 CCC: $30.25
Published on Web 07/26/2005

of four to 16 metal atoms, with certain exceptions such as Nb_8 and Nb_{10} which show much less reactivity. Computations of Roszak et al.[6] suggest that this effect is thermodynamic in origin.

Ethene chemistry is well characterized for neutral transition metal atom reactions in the gas-phase. Ritter et al.[19] have shown that, for first-row transition metal reactions with ethene under fast-flow reactor conditions, only Ni has a rate coefficient larger than the instrumentation limit for this experiment of 10^{-14} cm^3 s^{-1}. By comparison, late second-row transition metals react with ethene via third-body stabilized formation of π-complexes,[20] and early second-row transition metals react with ethene via bimolecular H_2-elimination reactions,[20,21] with Nb atoms showing the most pronounced reactivity (essentially at the gas-kinetic collision frequency). These results are in accord with the theoretical work of Blomberg et al.,[22] which shows a trend from π-complexation toward metallocyclopropane formation as the second-row transition metal series is crossed from late to early metals. Carroll and Weisshar[23] have also shown that several of the third-row transition metals also show significant reactivity with ethene. Wen et al.[24] have reported studies of Zr atoms reacting with ethene, and shown that the entire process of reaction to form a partially dehydrogenated product ZrC_2H_2 can occur with no barrier larger than 2 kJ mol^{-1}. Recently Porembski and Weisshar[25] have concluded from study of kinetic isotope effects that the reaction of Zr atoms with ethene proceeds via a molecular coordination followed by a C−H insertion step, and not a direct insertion into the C−H bond.

The chemistry of Nb cluster cations with ethene has been investigated by several groups, including Bondybey[9] and Freiser.[7,26] Jiao and Freiser[7] showed that sequential pick up of up to seven ethene molecules was observable for Nb_{13}^+, with a decreasing number of ethene monomers being picked up with decreasing cluster size. Extensive dehydrogenation is observed for all clusters studied. Notably low reactivity was again observed with Nb_8^+, Nb_{10}^+, and Nb_{12}^+, with significant variations in the saturation limits also seen. Interestingly, replacement of one Nb atom with a V atom effectively removes the nonreactive character of Nb_{12}^+ and to a lesser extent Nb_{10}^+, and replacement of one Nb with a Ta atom greatly minimizes the difference between 10 and 12 atom cluster cations and their nearest neighbors. Berg et al.[27] conclude that the low reactivity of Nb_{10}^+ and Nb_{12}^+ with ethene is a result of cluster structure, wherein the nonreactive cluster geometric isomer found for Nb_{10}^+ and Nb_{12}^+ is converted to a more reactive isomer by the replacement of one Nb atom with a V or Ta atom.

To date, relatively little is known about the reactivity of neutral metal clusters with ethene and other alkenes. We have therefore embarked on a detailed examination of the reactivity of metal clusters with this group of hydrocarbons. The present work on Nb cluster reactions with ethene is the first report on alkene reactivity in our fast-flow reactor apparatus, in which absolute rate coefficient determination is possible. It is also our first report to focus on the product mass observed over a wide range of cluster numbers, a focus which we believe is more fruitful for mechanistic insight than cluster removal rate analysis. The latter has been shown to be relatively insensitive to cluster size effects when the rate-determining step for cluster removal is a barrierless association process.[28] Such processes are expected to be common for highly polarizable metal clusters reacting with relatively complex reagents such as larger hydrocarbons. Absolute rate constants for cluster removal, as well as product mass data for primary, secondary, and subsequent products are reported. In conjunction with this work, density functional theory (DFT) calculations of Nb atom and Nb cluster reactions with ethene (up to Nb_6) are presented, the results of which are in remarkable accord with the observed patterns in extent of ethene dehydrogenation.

Experimental Section

The apparatus in the two configurations[29] used in this work has been described in detail[13,30] and therefore only a brief description is given here. Clusters are generated using a Smalley-type laser ablation source. A pulsed XeCl laser is focused onto a translating and rotating metal rod, over which a 15 000 standard cubic centimeter continuous flow of He (99.995% pure from Liquid Carbonics Inc.) is maintained, generating a metallic plasma which is entrained in the He flow. The He-plasma gas flows through a 1 cm-long, 0.2 cm diameter channel, where clusters are formed. Subsequently, the mixture expands into the large-bore (7.3 cm in diameter) flow tube reactor. In the presence of excess He bath gas the clusters equilibrate to flow tube temperature and pressure conditions before reaching the reaction zone.[11,31]

Flow tube pressure is varied in the range 0.5 to 2.2 Torr by partially closing the gate valve to the vacuum (600 Ls^{-1} Edwards EH2600 Rootes blower backed by an Edwards E1M275 mechanical pump). Data were collected at 300 K and at constant pressures ranging from 0.4 to 1.5 Torr. The specific temperature and pressure conditions used for various reported results are noted below.

Ethene (Matheson Research Grade 99.9%) is introduced through a shower-head inlet 60.6 cm downstream from the cluster source. Reagent gas pressure in the reactor is controlled by a mass flow controller (MKS model 1159). On reaching the end of the flow tube, the clusters and their reaction products pass into either an on-axis time-of-flight or a reflectron time-of-flight mass spectrometer (TOFMS) situated perpendicular to the flow tube axis. A pressure drop of approximately 6 orders of magnitude is maintained between the TOFMS and the flow tube by differential pumping, using an Edwards Diffstak 2300 L s^{-1} diffusion pump and an Edwards Diffstak 800 L s^{-1} diffusion pump in conjunction with an electromagnetic shutter used to reduce gas load. Clusters and reaction products entering the TOFMS are photoionized by a pulsed ArF laser operating at 193 nm that is triggered at a set delay with respect to firing of the ablation laser. The detector signal is digitized and sent to a personal computer for analysis. All mass spectra collected were averaged 200 (on-axis mass detection) or 500 times (off-axis detection).

Computational Details

Density functional theory (DFT) calculations were performed in order to find the most stable dehydrogenated products for the reaction between Nb atoms and Nb_n clusters ($n = 2-6$) and the ethene molecule. Theoretical results of the atom are included, despite the fact that the atomic energy is less accurately described by DFT than Nb clusters and molecular species containing one constituent Nb atom.[32]

All calculations were performed with Gaussian 98,[33] using the hybrid functional B3LYP,[34] LANL2DZ atomic orbital functions for Nb atoms (Hay and Wadt[35,36] effective core potentials plus a double-ζ basis set) and 6-311+G(2d,p)[37] for C and H atoms. Full geometry optimizations without symmetry constraints were carried out. Several initial geometries were used, as can be seen in Figure 1. For Nb_nC_2 we used the same niobium−carbon skeletons as $Nb_nC_2H_2$ (see Figure 1).

Several bond distances and angles were tested. Different spin multiplicities ($2S_z + 1$) were considered in all calculations in order to find the most stable spin state. To find the global minimum, one must consider several multiplicities and several initial structures for each adduct. The possibility that the true

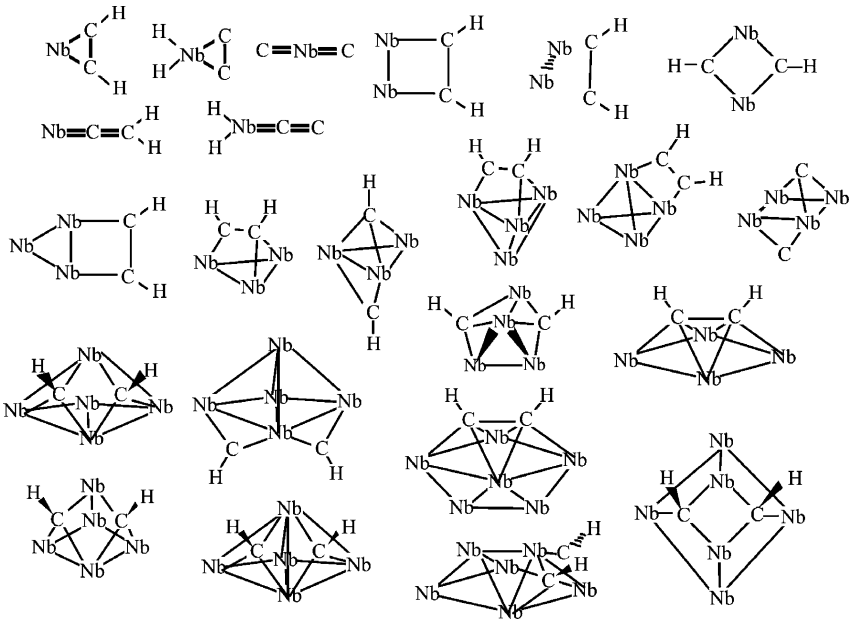

Figure 1. Initial structures used in $Nb_nC_2H_2$ and Nb_nC_2 geometry optimization calculations.

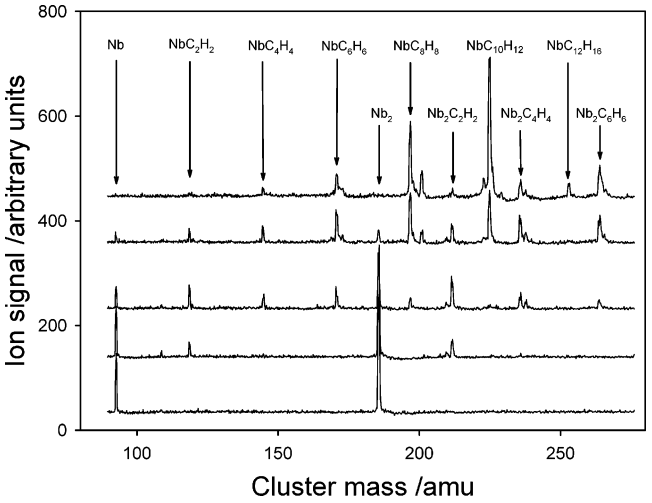

Figure 2. Mass spectra in the mass range of Nb and Nb_2 showing the effect of introducing ethene into the flow tube. Reagent flows in ascending spectral order are: no added reagent (bottom spectrum), 0.005, 0.02, 0.05, and 0.1 mTorr of ethene added (top spectrum). Major product peaks formed after formal addition of ethene are noted, with their empirical formula for the peak center mass.

global minimum was missed in the optimization procedure cannot be excluded, but the number of different initial geometries and spin multiplicities that were considered is sufficiently high to feel confident that the global minimum has been identified. Optimized minima were verified with frequency calculations. Gibbs energies (ΔG) and enthalpies (ΔH) for the reactions at 298.15 K and 1 atm were also calculated. The corrections were made using the ideal gas approximation in a canonical ensemble. All figures were done with Ball & Stick and MOLEKEL.[38]

Results

Nb atoms and clusters up to Nb_{25} were observed to react readily with ethene, based upon the depletion of TOF mass spectrometric signals for these species with increasing ethene pressure in the flow reactor. Representative mass spectra are shown in Figure 2 for data collected for Nb atoms and Nb_2 at 1 Torr total flow reactor pressure.

With most clusters, product peaks reflecting sequential addition of ethene or dehydrogenated ethene can be clearly seen. Figure 2 shows the sequential growth of products corresponding to addition of six units of ethene to Nb and three units to Nb_2. For the products that are observed, the occurrence of some post-ionization dehydrogenation cannot be ruled out in light of the fact that Nb cluster cations are also known to dehydrogenate hydrocarbons.[9,16,26]

By monitoring the rate of cluster depletion as a function of reagent number density, absolute second-order rate coefficients for cluster depletion were obtained. Assuming that the reagent gas is in sufficient excess, the pseudo first-order kinetics expression appropriate for atom or cluster depletion is

$$\ln\left(\frac{I}{I_0}\right) = -k^{(2)}[C_2H_4]\tau$$

where I and I_0 are the mass spectral peak intensities in the presence and absence of reagent gas, respectively, $[C_2H_4]$ is the ethene number density in the flow tube, τ is the reactant contact time,[39] and $k^{(2)}$ is the absolute second-order rate coefficient ($cm^3\ s^{-1}$). All pseudo first-order kinetics plots were linear as typified in Figure 3 by the reaction of Nb_5.

The rate coefficients calculated from the slopes of such plots are presented in Table 1 and plotted in Figure 4, which shows a generally smooth increases in the rate coefficients as the number of constituent Nb atoms increases.

Exceptions to this trend are Nb_8 and Nb_{10}, for which rate constants of about 1 order of magnitude smaller are observed. The extent of cluster depletions, and hence the rate coefficients determined, was not sensitive to ionization laser fluence, indicating that the experiments were conducted under conditions of single-photon ionization. Rate coefficients for all species except for Nb_8 and Nb_{10} showed no obvious dependence on total flow tube pressure between 0.5 and 3 Torr as demonstrated by the representative data given for Nb_5 at pressures between 0.4 and 1.0 Torr illustrated in Figure 3.

Associated with the depletion of all observed Nb species are product features that correspond to cluster reactions with ethene molecules. The observed masses indicate that dehydrogenation occurs to varying degrees, both as a function of cluster size, and as a function of how many ethene molecules have reacted.

In Figure 5 is illustrated the mass of product observed as a function of cluster size for the primary, secondary and tertiary

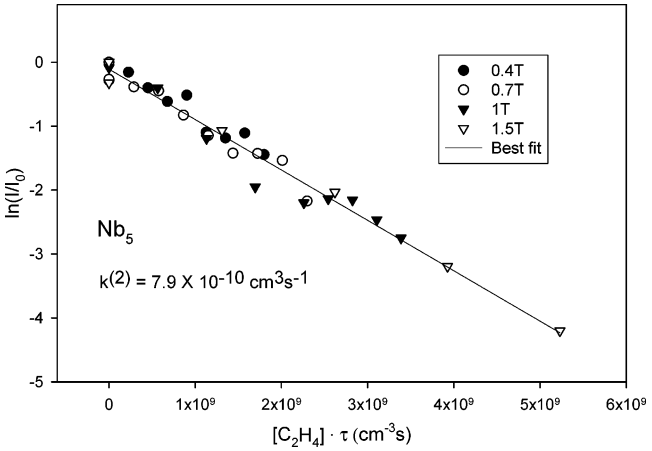

Figure 3. Representative pseudo-first-order kinetics plot used to determine absolute second-order rate coefficients for Nb_5 reactions with ethene. Plotted together are data for total flow tube pressures of 0.4 (filled circle), 0.7 (open circle), 1.0 (filled triangle), and 1.5 Torr (open triangle), to demonstrate the absence of total pressure dependence of rate coefficient. Solid line is the regression line of best fit.

TABLE 1: Absolute Second-Order Rate Coefficients $k^{(2)}$ for the Removal of Nb Clusters by Ethene at 300 K and 1 Torr (10^{-10} cm^3 s^{-1}),[a] and Corresponding Major[b] Product Fragment Masses (amu) for Observed Primary, Secondary, and Tertiary Products

		product mass		
n	$k^{(2)}$	primary	secondary	tertiary
1	2.7	26	52	78
2	4.0	26	52	78
3	7.1	26 *(24)*	52 *(50)*	78
4	7.1	24	52	78
5	6.4	24	50	78
6	7.3	24	50	76
7	6.5	24	50	76
8	1.74	26	50	76
9	8.1	26	52	76
10	1.28	28	56	82
11	10.1	26	52	
12	6.6	26	50	76
13	12.4	24	50	74
14	11.4	26	50	
15	13.9	26	52	78
16	11.0	26	50−54	
17	13.2	26	52	
18	14.7	26	54	
19	13.0	26	50	
20	14.1	26		
21	17.8	26		
22	17.1	26		
23	16.5	26		
24	20.6	26		
25	21.0	26		

[a] Rate coefficients are estimated to be accurate to within 50% (see ref 31) [b] Where present, minor products and shoulders appearing in mass spectra are recorded in italics.

products, where the mass of the observed product is known with confidence. The data show a general trend toward increased dehydrogenation with cluster size up to Nb_7. All Nb clusters, save Nb_{10}, yield primary, and, where observed, secondary, and tertiary products for which loss of at least one unit of H_2 is evident. Where observed, formal addition of C_2H_4 is generally observed for products formed sequentially beyond this point. For example, addition of ethene to Nb_2 beyond the tertiary product is observed to correspond to addition of a hydrocarbon unit with mass corresponding to C_2H_4. Table 2 gives the product masses observed beyond tertiary for Nb atoms and several small Nb clusters.

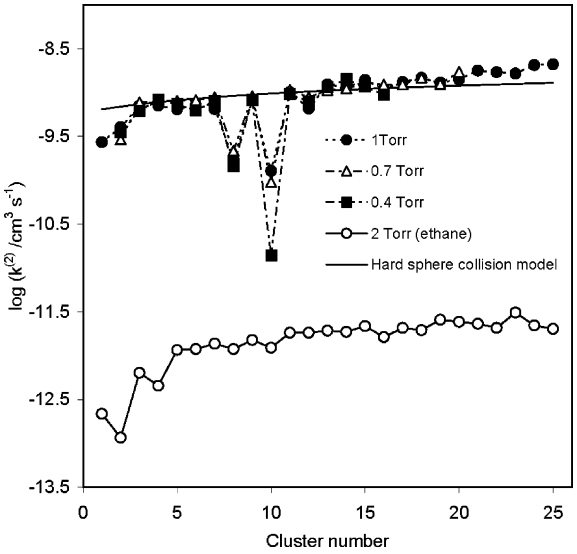

Figure 4. Rate coefficients for the reactions of Nb_n with ethene plotted against cluster number for total flow tube pressures of 0.4 (filled square), 0.7 (open triangle) and 1.0 Torr (filled circle). Solid curve is the calculated gas-kinetic collision rate, based upon approximation of the clusters and ethene as hard spheres. Also plotted are rate coefficients for the removal of Nb clusters by ethane, for comparison.

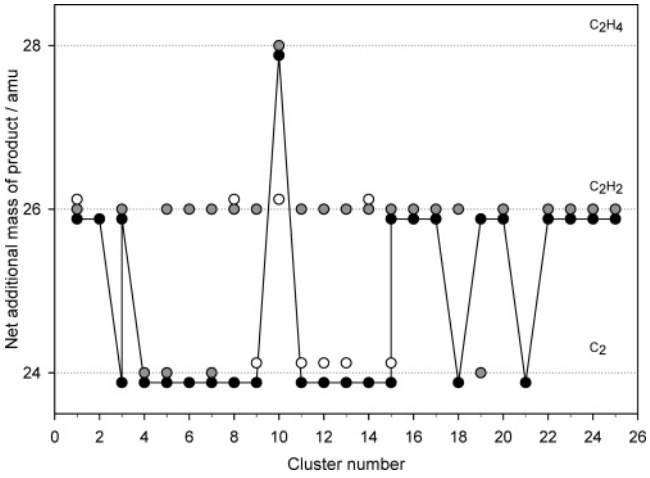

Figure 5. Graphical representation of the mass of primary (filled circles), secondary (shaded circles) and tertiary (open circles) products (where observed) for Nb atoms and clusters from Nb_2 to Nb_{26}. Where more than one symbol appears for a given cluster, two products are observed. Solid line joins the observed primary products. Primary and tertiary product masses have been offset slightly for clarity.

Detailed kinetic analysis of the growth-and-decay behavior of the various product peaks was carried out for several clusters and the Nb atom, using standard equations for *n* irreversible, sequential reactions.[40]

$$R + M \xrightarrow{k_1} MR \quad (1)$$

$$R + MR \xrightarrow{k_2} MR_2 \quad (2)$$

$$R + M \xrightarrow{k_3} MR_3 \quad (3)$$

$$\cdots$$

$$R + M \xrightarrow{k_n} MR_n \quad (n)$$

All showed well-behaved, sequential formal addition of ethene, with rate coefficients as summarized in Table 3 and illustrated in Figure 6.

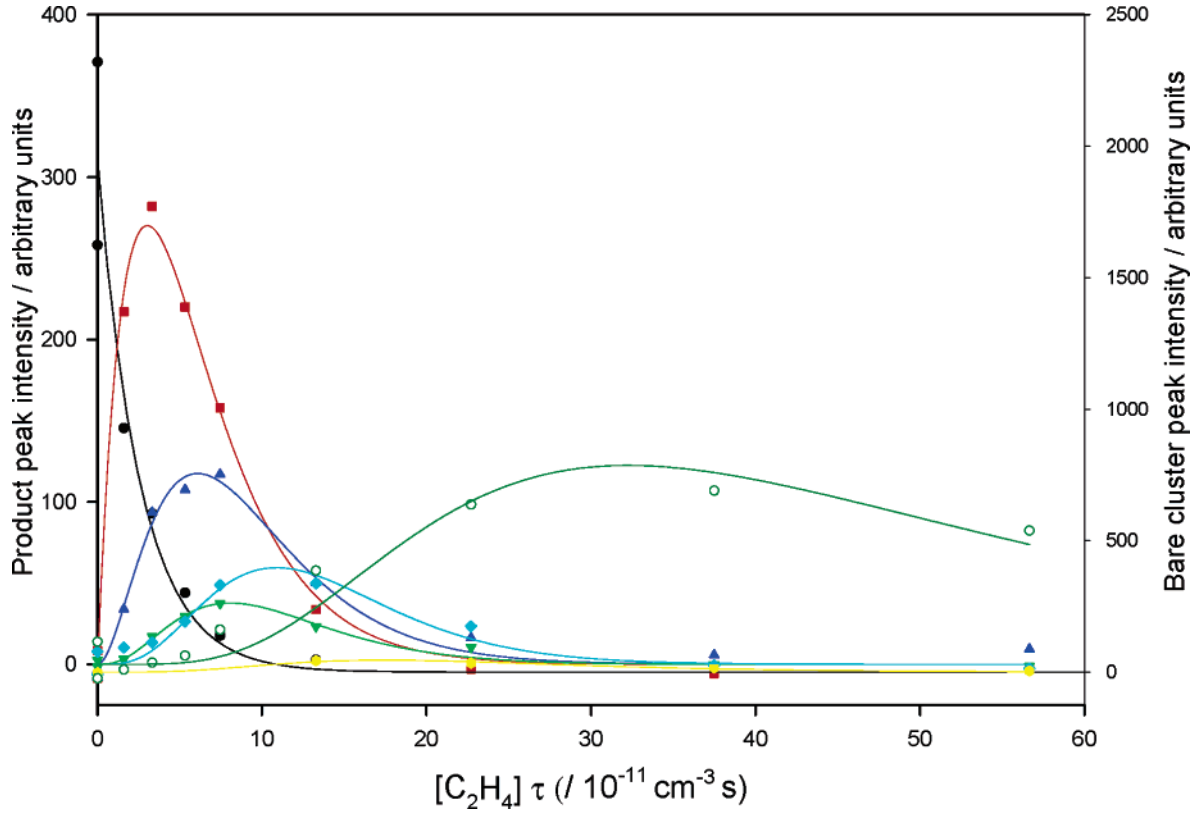

Figure 6. Illustration of product growth-and-decay behavior for the Nb_5 reaction with ethene. Data are given for the bare Nb_5 cluster removal (black), and growth and decay of the primary (red), secondary (blue), tertiary (green), quaternary (aqua), and quinary products (olive). Solid lines illustrate the fit with a model involving sequential pick up of ethene molecules.

TABLE 2: Primary, Secondary and Tertiary Product Masses Differences for Formal Addition of Ethene Molecules to Nb Clusters for Various Cluster Numbers[a]

n	primary	secondary	tertiary	quarternary	quinary	senary
1	26	26 (52)	26 (78)	26, *30* (104, *108*)	28 (132, *136*)	28, *24* (160)
2	26	26 (52)	26 (78)	28 (106)	28 (134)	28 (162)
3	26, *24*[b]	26 (52, *50*)	26 (78)			
4	24	28 (52)	26 (78)			
5	24	26 (50)	28 (78)	28 (104)	28 (132)	28 (160)
6	24	26 (50)	26 (76)	28 (104)	28 (132)	26, 28 (158)
7	24	26 (50)	26 (76)			
8	26	24 (50)	26 (76)			

[a] Where observed, masses for subsequent products are also reported. Masses in parentheses indicate total product mass recorded. [b] Data in italics reflect shoulder or minor peaks in mass spectra, and related mass differences.

Theoretical Results

1. Bare Nb Clusters (Nb_n). The geometries obtained for the bare Nb clusters are in good agreement with those previously reported[2−4] as shown in Table 4, with the exception of Nb_3 where we found an isosceles triangle with bond distances of 2.35, 2.35, and 2.47 Å, while other authors[2,3] reported also an isosceles triangle but with two long sides. We also found an isosceles triangle with sides 2.29, 2.44, and 2.44 that lies 0.8 kJ mol^{-1} higher in energy. The energy difference between these two triangles is very small, and does not affect the general conclusions about the chemical reactivity of these clusters.

The vertical ionization energies (IP) for Nb_2−Nb_6 are shown in Table 5, and compared with the experimental vertical ionization energies reported by Knickelbein and Yang.[41] There is a good agreement between theoretical and experimental values. Note that the calculated IP for the Nb atom shows an error of about 1 eV, and is therefore not included in this table.[32] With this theoretical description of the Nb clusters, it is possible to study the reactivity behavior of these systems with ethene. As well, the reactivity of the atom may be investigated theoretically, although with more significant associated error.

TABLE 3: Rate Coefficients for Removal of Various Products in the Reaction of Nb_5 Clusters with Ethene, Obtained from a Sequential Bimolecular Reaction Model Analysis of the Growth and Decay Behavior of the Metal Species and Observed Products

	reaction rate coeff/10^{-10} cm^3 s^{-1}		
reacting species	Nb	Nb_2[b]	Nb_5
bare cluster[a]	3.5	4.8	9.3
primary product	5.2	3.8	6.7
secondary product	6.3	9.6	7.9
tertiary product	9.2	2.6	13.0
quaternary product	2.2	1.7	8.5
quinary product	0.73	1.1	2.4
senary product	0.79	1.8	0.87

[a] Rate coefficients for the bare clusters and all product reaction rate coefficients were calculated using a direct exponential fit, not involving linearization as was used in the calculation of bare cluster depletion rates. As a result the rate coefficients obtained for the bare species differ slightly from those reported in Table 1, particularly for Nb_5 for which signal-to-noise was somewhat elevated. [b] Data obtained for Nb_2 has a significantly lower signal-to-noise ratio than Nb and Nb_5. As a result the values given here for Nb_2 have higher associated error.

TABLE 4: Structure, Bond Distance in Å and Spin Multiplicity ($2S_z+1$) for Bare Niobium Clusters Calculated in This Work[a]

Structure	$2S_z+1$	Kumar and Kawazoe[2] ultrasoft pseudopotential method	Goodwin and Salahub[3]	Grönbeck and Rosen [4] LSDA
Nb_2 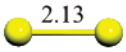	3	triplet, 2.15	triplet, 2.10	triplet, 2.11
Nb_3 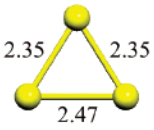	2	isosceles triangle, doublet, 2.42, 2.42, 2.29	isosceles triangle, doublet, 2.37, 2.37, 2.26	acute triangle, doublet, 2.40, 2.25
Nb_4 	1	tetrahedron, singlet, 2.53	tetrahedron, singlet, 2.47	slightly distorted tetrahedron singlet, 2.51, 2.52
Nb_5 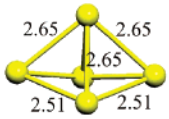	2	capped bent rhombus, doublet, 2.48 rhombus side	trigonal bipyramid, doublet, equatorial bonds 2.71, polar-equatorial bonds 2.43	trigonal bipyramid, doublet, equatorial bonds 2.77, polar-equatorial bonds 2.46
Nb_6 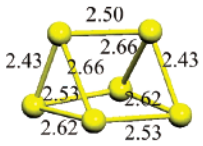	1	distorted prism, singlet, bond range 2.42-2.94	parallelepiped capped with a dimer, singlet	parallelepiped capped with a dimer, singlet

[a] Previous results are also shown.

TABLE 5: Calculated Vertical Ionization Energies for the Bare Clusters

cluster	cation multiplicity	calculated IPs (eV)	experimental IPs[41] (eV)
Nb_2	4	6.5	6.2 ± 0.1
Nb_3	3	5.91	5.81 ± 0.05
Nb_4	2	5.59	5.64 ± 0.05
Nb_5	1	5.54	5.45 ± 0.05
Nb_6	2	5.36	5.38 ± 0.05

2. Optimized Structures of $Nb_nC_2H_2$ and Nb_nC_2. The most stable structures of $Nb_nC_2H_2$ and Nb_nC_2 ($n = 1-6$) are shown in Figure 7.

All the systems present the lowest spin multiplicity, with the exception of NbC_2H_2 and NbC_2, which are predicted to be quartets, with C_{2v} symmetry. For these species, the C−C bond distances indicate that there is a double bond between the C atoms (1.33 and 1.31 Å, respectively). $Nb_2C_2H_2$ and Nb_2C_2 are singlets, with C_{2v} symmetry. The C−C bond lengths (not shown in Figure 7) are 2.95 and 2.72 Å, indicating that the C−C bond of ethene is broken. For the dimer, the Nb−C bond lengths are very different, and generally the hydrogen-containing compounds show consistently longer Nb−C bond lengths than those without hydrogen. Nb_2C_2 shows the smallest Nb−C bond distance (1.91 Å) of all the systems. As well, the C−H bond lengths $Nb_nC_2H_2$ show a small increase with cluster size, going from 1.087 (NbC_2H_2) to 1.106 Å ($Nb_6C_2H_2$).[42] For comparison, note that our computations yield a C−C bond distance of 1.325 Å and the C−H bond distance of 1.084 Å for free ethene.

$Nb_3C_2H_2$ and Nb_3C_2 are doublets and have C_{2v} symmetry (see Figure 7). The Nb trimer shows the same arrangement after reaction (isosceles triangle) as in the bare cluster. $Nb_4C_2H_2$ and Nb_4C_2 are singlets. The calculated cluster structures undergo several changes on reaction, with some Nb−Nb bonds broken in order to form six Nb−C bonds. In both compounds, we have two different Nb−C bond distances (2.05 and 2.20 Å for $Nb_4C_2H_2$; 1.94 and 2.03 Å for Nb_4C_2). $Nb_5C_2H_2$ and Nb_5C_2 are doublets and have C_s symmetry; $Nb_6C_2H_2$ and Nb_6C_2 are singlets with C_{2v} symmetry, as shown in Figure 7. The Nb−C bond distances are similar to those in the other systems.

With these results it is possible to predict that $Nb_nC_2H_2$ and Nb_nC_2 present the same symmetry and general structure, with different bond distances. In general, Nb_nC_2 cluster geometries exhibit shorter Nb−C bonds distances than $Nb_nC_2H_2$ clusters, with a

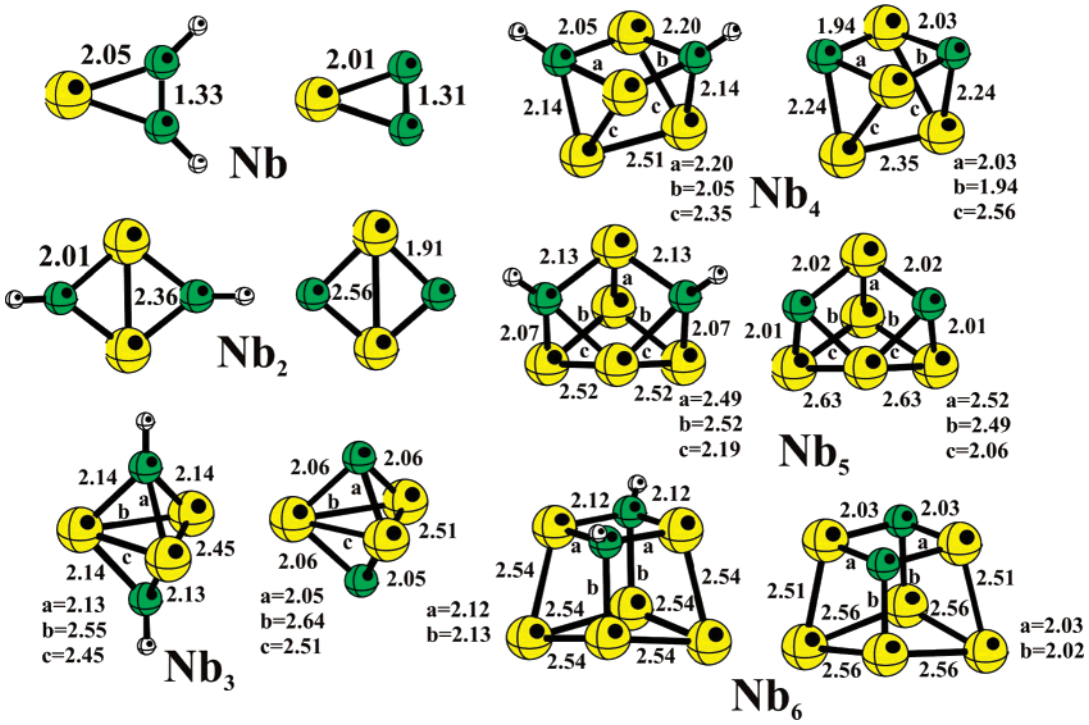

Figure 7. Optimized minimum-energy structures for $Nb_nC_2H_2$ and Nb_nC_2 species. Bond distances are in Å.

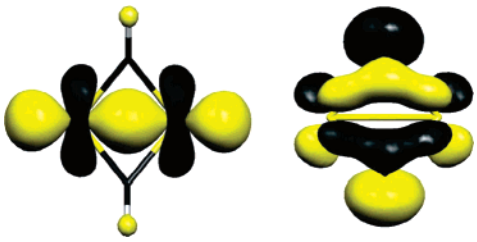

Figure 8. Molecular orbital images for $Nb_2C_2H_2$ and Nb_2C_2. The illustrated orbital is the second highest occupied molecular orbital (HOMO-1).

few exceptions. On the other hand, calculated Nb−Nb bond lengths are generally longer in Nb_nC_2 than in $Nb_nC_2H_2$ ($n = 2...6$).

Figure 8 shows the molecular orbital images of $Nb_2C_2H_2$ and Nb_2C_2. The illustrated orbital is the second highest occupied molecular orbital (HOMO-1) and it is the only orbital that shows a significant difference between both compounds. For $Nb_2C_2H_2$, this orbital shows σ−bonding character between the Nb atoms, i.e., a two-center, two-electron bond, which would be expected to result in a strong Nb−Nb bond. For Nb_2C_2, the corresponding orbital shows a π-bonding network over the Nb−C−Nb framework, i.e., a four-center, two-electron bond, which would be expected to favor Nb−C bonding. This significant difference in bonding between theses two species is likely the main reason for the calculated Nb−Nb distance in $Nb_2C_2H_2$ being significantly shorter than that of Nb_2C_2.

3. Reactivity. The sequential nature of the ethene reactivity indicates that the reaction steps following the initial ethene pick up step must be fast and unimolecular. Therefore, the analysis is focused on the most likely mechanism for formal dehydrogenation of ethene, which leads to the elimination of molecular hydrogen. The overall reactions are

$$Nb_n + C_2H_4 \rightarrow Nb_nC_2H_2 + H_2 \quad \text{first dehydrogenation step}$$

$$Nb_nC_2H_2 \rightarrow Nb_nC_2 + H_2 \quad \text{second dehydrogenation step}$$

$$Nb_n + C_2H_4 \rightarrow Nb_nC_2 + 2H_2 \quad \text{overall process}$$

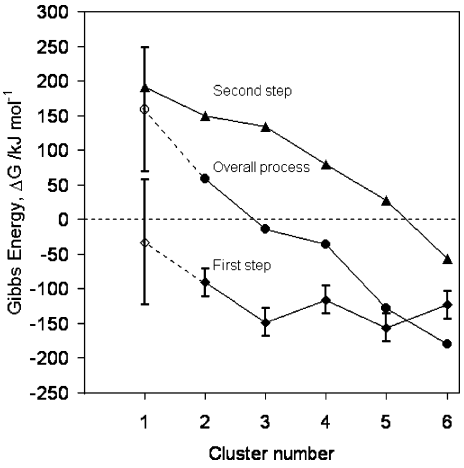

Figure 9. Plots of the variation in predicted Gibbs energy of reaction with cluster size from Nb to Nb_6, for the first, second and total dehydrogenation processes involving production of molecular hydrogen. Note that the error associated with predictions involving the free Nb atom is significantly larger than that for all other species, as discussed in the text.

Table 6 shows the reaction energy (ΔE), enthalpies (ΔH), and Gibbs energy changes (ΔG) at 298.15 K and 1 atm for the first, second, and overall dehydrogenation reactions involving production of H_2. The same information for the Gibbs energy change associated with each step is represented graphically in Figure 9.

Figure 9 demonstrates that production of the partially dehydrogenated product $Nb_nC_2H_2$ is predicted to be exergonic for all clusters studied (Nb_2−Nb_6). The Nb atom result follows this trend, however, there is much more error associated with the calculation of Nb, such that the process could be predicted to be either endergonic or exergonic. In contrast, the second dehydrogenation step is endergonic for all species studied save $Nb_6C_2H_2$. Coupling of the two processes in the production of fully dehydrogenated ethene is predicted to be thermodynamically favored for Nb_4–Nb_6, thermoneutral for Nb_3, and ender-

TABLE 6: Predicted Values for ΔE, ΔH, and ΔG at 298.15 K and 1 atm for the First, Second, and Overall Total Dehydrogenation of Ethene To Form Molecular Hydrogen by Nb_n Species (n = 1 to 6) with All Values in kJ mol^{-1}

	$Nb_n + C_2H_4 \rightarrow Nb_nC_2H_2 + H_2$			$Nb_nC_2H_2 \rightarrow Nb_nC_2 + H_2$			$Nb_n + C_2H_4 \rightarrow Nb_nC_2 + 2\ H_2$		
n	ΔE	ΔH	ΔG	ΔE	ΔH	ΔG	ΔE	ΔH	ΔG
1	−3.3	−33.5	−33.1	253.6	229.7	191.6	250.2	196.2	158.6
2	−69.9	−102.9	−90.8	203.8	185.8	149.0	133.9	82.8	58.2
3	−138.1	−169.5	−148.5	192.0	172.0	134.3	54.0	2.5	−14.2
4	−96.7	−131.0	−115.9	132.6	116.7	79.5	36.0	−14.2	−36.4
5	−147.7	−182.8	−156.1	75.7	61.9	28.0	−72.0	−120.9	−128.0
6	−110.9	−146.0	−123.0	−10.9	−24.3	−56.5	−121.8	−170.3	−179.5

gonic for Nb and Nb_2. This final set of theoretical predictions is in excellent agreement with the observed experimental trend (see discussion below).

Discussion

The results of the present work show that Nb clusters react readily with ethene in the gas phase to form products that correspond formally to partial or full dehydrogenation of ethene. All clusters react with rate coefficients approximately equal to the gas-kinetic collision frequency, with the exception of Nb_8 and Nb_{10}, for which significantly decreased rate coefficients are observed. Many clusters show sequential reactions of ethene monomers with kinetics that correspond to pseudo-first-order processes with rate coefficients close to the gas-kinetic collision rate coefficient.

The low rate coefficients for Nb_8 and Nb_{10} are in accord with previous results for reactions of Nb clusters with several molecular species. As noted above, Nb clusters exhibit significant cluster-size selectivity, with particularly low reactivity noted for Nb_8, Nb_{10}, and Nb_{16} with D_2 and N_2.[11] Absolute rate coefficient measurement by Berces et al.[14] show that the most reactive clusters have probabilities of a reactive collision of the order of 0.1, in accord with the high rate coefficients found here with ethene. Their work demonstrated that the low reactivity of Nb_8, Nb_{10}, and Nb_{16} could be associated with maxima in the ionization potential for the cluster, when corrected for cluster electrostatic charging energy. Kumar et al.[2] have also recently computed large HOMO−LUMO energy gaps for Nb_6, Nb_8, Nb_{10}, and Nb_{16}, which may also cause reduced reactivity. Thus, the observation of low rate coefficients for Nb_8 and Nb_{10} in the present work suggests that the same interactions are present in the ethene chemistry that control selectivity with D_2 and N_2, namely charge transfer between the cluster and ethene, as would be expected for traditional bonding of ethene at a metal center. It is therefore likely that the first mechanistic step is association of ethene to form a π-bonded complex at the metal. The pressure dependence of Nb_8 and Nb_{10} reflects a mechanism for removal that most likely involves reversible π-complexation, indicating unusually weak interaction between the cluster and ethene.

The excellent fit of the kinetics of product formation and consumption to a pseudo-first-order sequential addition model, and the high rate coefficients obtained, strongly suggest that barrierless association complex formation is the rate-limiting step in all of the subsequent reactions of primary and subsequent products with ethene. Siegbahn et al.[43] have calculated the activation of ethene to form vinylmetal hydrides, and predict them to be exoergic for early transition metals including Nb atoms, such that barrierless steps leading to cluster hydride species are also possible. For the first two or three addition steps, there is a general trend toward increased reaction rate constant with each subsequent addition, which is likely to be due to increase in extensive factors such as polarizability and collision cross-section.

Such sequential reaction behavior has been observed in previous work with cluster cations, in which cluster-mediated production of benzene from ethene has been observed. Schnabel et al.[44] showed that Fe_4^+ ions convert ethene to benzene in a catalytic cycle, in which CID experiments show release of C_6H_6 species believed to be benzene. Berg et al.[45] showed that W^+ ions can add up to nine ethene molecules, with CID experiments also showing desorption of fragments corresponding to C_6H_6. The kinetics of sequential ethene addition was also studied in their work. Application of a sequential, pseudo-first-order reaction kinetics model showed rate coefficients corresponding to the gas-kinetic collision rate for the first four additions, with the subsequent five additions occurring with rate coefficients of about 0.2 of this value. The decreased extent of dehydrogenation of the quaternary and subsequent products in this work may reflect the blocking of active surface sites on the cluster, due to the presence of coordinated benzene, formed following the first three ethene addition steps.

The more interesting variations in chemical reactivity with cluster size are found in the masses of primary and subsequent products. The degree of dehydrogenation for primary products is most pronounced for clusters between Nb_4 and Nb_{15}, with the exception of Nb_{10} for which no dehydrogenated primary product is observed. The same trend toward relatively increased degree of dehydrogenation in this cluster mass range is seen with secondary and tertiary products, although the extent of dehydrogenation is less for these products. The tendency toward increased dehydrogenation from Nb to Nb_6 is supported by the computational results presented above, which suggest strongly that the thermodynamics of complete dehydrogenation becomes more favorable as the cluster size increases, as discussed below.

Zakin et al.[15,16] also showed that product mass dependence on cluster size is present with neutral Nb clusters and cluster cations in reactions with benzene. In this work, significant benzene dehydrogenation up to complete loss of all hydrogen for clusters Nb_4−Nb_7 was observed, with some dependence of the extent of dehydrogenation on ionization energy for the neutral species. Clusters Nb_8−Nb_{10} showed a notable lack of dehydrogenation, yielding C_6H_6 adducts as reaction products. Simultaneously reported work on Nb neutral clusters by St. Pierre et al.[17] showed minima in the extent of dehydrogenation efficiency for Nb_8, Nb_{10}, and clusters smaller than Nb_4. In contrast to this, ICR work of Berg et al.[18] has demonstrated that dehydrogenation efficiency for Nb cluster cations shows a maximum in the size range 7−14, with incomplete dehydrogenation for small and larger cluster cations. Such a trend has also been observed for small Nb cluster cations with propene and 1-butene by Jiao et al.[8] As noted above, computations of Roszak et al.[6] indicate that this effect is thermodynamic in origin, the dehydrogenation steps being more endoergic for smaller clusters. The discrepancy between the work of the Bondybey group in the ICR, and the earlier cluster work appears to be due to differences in the effective cluster temperature, which is significantly lower in the ICR experiment.

The theoretical work presented here is in good accord with the proposal that the dehydrogenation processes occurring in the present work involve production of molecular hydrogen. The data presented in Table 6 and Figure 9 show that partial dehydrogenation of C_2H_4 by Nb_n ($n = 2...6$), forming NbC_2H_2, is exergonic. It is not possible to confidently predict the thermochemistry of the partial dehydrogenation reaction of ethene with the Nb atom, due to the large error in the calculated Nb atom energy. However, the predicted value does fall in line with the trend found for the small cluster species, and is in agreement with the experimental observation of NbC_2H_2 as the only dehydrogenation product for the Nb atom reaction (see below). The production of fully dehydrogenated ethene to form Nb_nC_2 from $Nb_nC_2H_2$ is predicted to be thermodynamically favored only for Nb_6. Full dehydrogenation to form Nb_nC_2 from $Nb_n + C_2H_4$ is predicted to be exergonic for Nb_4–Nb_6, thermoneutral for Nb_3, and endergonic for Nb and Nb_2. However, given that the second dehydrogenation step is endergonic for all but Nb_6, the full dehydrogenation process can only occur for Nb_n ($n = 3...6$), if the Gibbs energy released in the first partial dehydrogenation step were available for the subsequent unimolecular decomposition of the proposed $Nb_nC_2H_2$ intermediate. This would imply that the energy released in the first dehydrogenation step is not lost to collisions with the bath gas before the intermediate decomposes to the carbidic Nb_nC_2 species and molecular hydrogen. The fact that the observed pattern of reactivity for the Nb atom and clusters from Nb_2 to Nb_6 matches exactly the thermodynamic product distribution predicted from the theoretical calculations suggests that such thermalization is not occurring, and that the reaction proceeds via molecular hydrogen formation. Thus, Nb_2, for which the overall dehydrogenation process is endergonic by 58.2 kJ mol^{-1} yields only the thermodynamically favored $Nb_2C_2H_2$ species. Nb_3, for which the overall dehydrogenation process is approximately thermoneutral[46] produces both $Nb_3C_2H_2$ and Nb_3C_2, and the clusters Nb_4–Nb_6, for which the overall dehydrogenation reaction is significantly exergonic, produce only the fully dehydrogenated Nb_nC_2 products.

It is of significant interest to determine the structural or chemical origin of the thermodynamically determined trend in the extent of dehydrogenation of ethene with cluster size for small clusters. The theoretical computations presented here support the conclusion that complete ethene dehydrogenation becomes more favorable as the cluster size increases from Nb to Nb_6. Analysis of the optimized structures of the various cluster geometries, which we believe to represent the global structural minima for the various clusters studied, shows that the only systematic structural trend that follows the increase in reaction exergonicity is the length of the C–H bonds in the C–H fragments of $Nb_nC_2H_2$ species.[47] We note that the C–H bonds become systematically longer as the cluster size varies from NbC_2H_2 to $Nb_6C_2H_2$.

It can be easily shown that there is a very good correlation between C–H bond length and C–H bond dissociation energy (BDE), as can be demonstrated by correlating data for methane, ethane, ethene and ethyne from published data,[48] as shown in Figure 10.

Such a correlation yields the following linear relationship that may be used to estimate the BDE for hydrocarbon fragments in the cluster species:

$$(\text{C–H BDE /kJ mol}^{-1}) = -3107.5 \times (\text{C–H bond length /Å}) + 3840.5$$

with a correlation coefficientof $R^2 = 0.8894$. Using this relationship, we have estimated the C–H bond dissociation energies based upon their calculated C–H bond length values, for the Nb_n species containing C_2H_2 fragments, and examined the relationship between the weakening of the C–H bond and the change in Gibbs energy of reaction. Figure 11 shows this relationship; the best-fit regression line has a regression coefficient of $R^2 = 0.9814$.

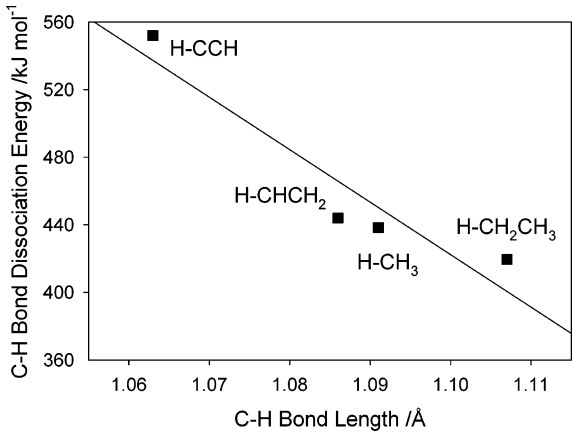

Figure 10. Plot of the correlation between C–H bond dissociation energy (kJ mol^{-1}) and C–H bond length (Å) for four hydrocarbons. Regression line corresponds to the equation given in the text.

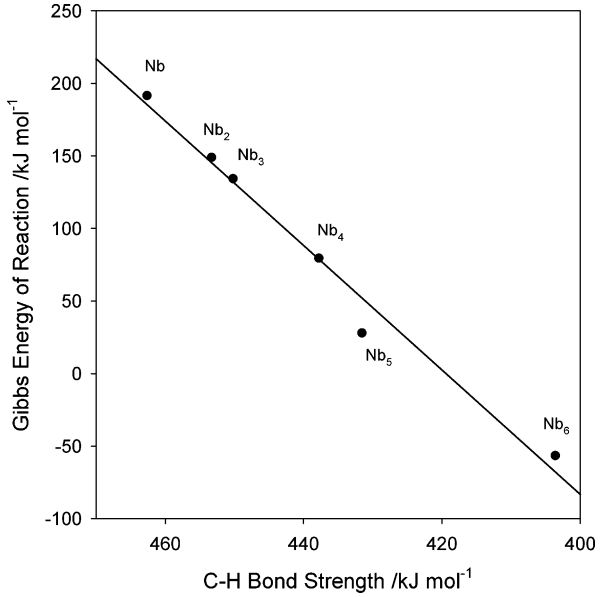

Figure 11. Plot of the relationship between Gibbs energy of reaction for total dehydrogenation of ethene to form H_2 vs the calculated strength of the C–H bond in the partially dehydrogenated species $Nb_nC_2H_2$. Solid line corresponds to the regression equation given in the text.

The linear relationship in Figure 11 strongly supports the notion that the weakening of the C–H bond in $Nb_nC_2H_2$ species leads to increased exergonicity associated with its subsequent dehydrogenation to form Nb_nC_2. It is likely that the decrease in C–H BDE with cluster size is due to the increasing polarizability of the metal clusters which increases the extent of charge flow to the electron-poor carbon of the C–H fragments, resulting in a weakened C–H bond. In a sense, the carbon of the C–H fragment becomes more carbidic in nature as the cluster increases in size and polarizability. We anticipate that such an effect should be found for all hydrocarbon dehydrogenation processes involving C–H fragments in the mechanism, and indeed have seen similar trends in extent of dehydrogenation with other hydrocarbons such as propene and butene.

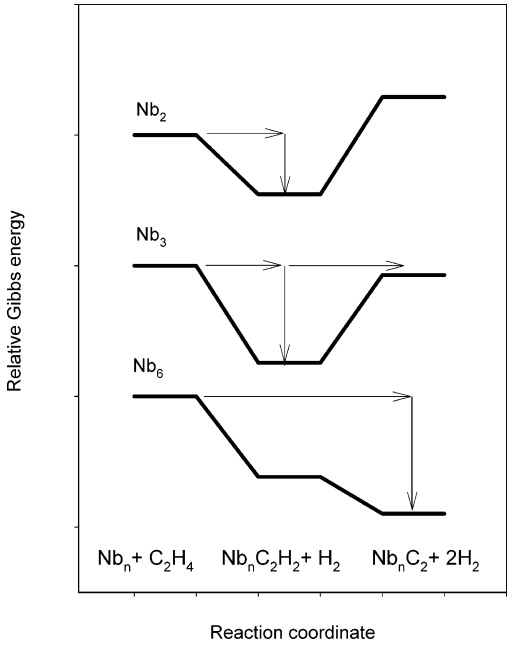

Figure 12. Predicted Gibbs energy changes for the dehydrogenation of ethene by Nb_2, Nb_3, and Nb_6 clusters, relative to $Nb_n + C_2H_4$. Horizontal arrows indicate movement along reaction coordinate, vertical arrows indicate relaxation following collisional energy transfer.

The experimental observation of both the partially and fully dehydrogenated products with Nb_3 demonstrates that the second dehydrogenation step must be essentially barrierless. Vibrational relaxation of the initially formed energized $Nb_3C_2H_2$* species to form relaxed $Nb_3C_2H_2$ would then be in competition with unimolecular decomposition to form Nb_3C_2 and H_2, yielding both products. Given that the morphology of the potential energy surfaces for the unimolecular decomposition of $Nb_nC_2H_2$ intermediates is expected to be similar from one cluster to the next, the absence of a barrier for Nb_3 implies the same condition for all other clusters. We would therefore expect no significant barriers beyond the endergonicity of the process for the second decomposition step in all clusters.

Figure 12 illustrates the conclusions that can be drawn from these points. For Nb_2, the endergonicity of formation of Nb_2C_2 from $Nb_2C_2H_2$ exceeds the energy available from the prior formation of $Nb_2C_2H_2$. Hence only the partially dehydrogenated product is observed, following relaxation from energy transfer to He collision partners. For Nb_3, the production of the fully dehydrogenated product is endergonic by about the same amount of Gibbs energy released in the first step, hence both the partially and fully dehydrogenated products are observed, reflecting competition between collisional relaxation and unimolecular decomposition processes. For Nb_6, the reaction to form Nb_6C_2 is fully exergonic in both steps, and can proceed directly to products without any barrier. Note that for Nb_4 and Nb_5 (not illustrated), the Gibbs energy released in the first step significantly exceeds the endergonicity of the second step, resulting in efficient production of the fully dehydrogenated Nb_nC_2 species.

It is interesting to note that clusters larger than Nb_6 show a trend toward production of the partially dehydrogenated $Nb_nC_2H_2$ species. Since there is no reason to anticipate that the weakening of the C−H bond of CH fragments in the partially dehydrogenated cluster species would reverse as clusters become larger and more polarizable, we would predict that other thermodynamic or kinetic factors are coming into play as the clusters grow in size that influence the product distribution observed. Such an effect may be associated with the increasing separation of CH fragments on the cluster surface, which make production of the thermodynamic product impossible due to kinetic constraints on the unimolecular decomposition of $Nb_nC_2H_2$.

Conclusions

The reactions of Nb clusters with ethene lead to partially or fully dehydrogenated products via a sequential ethene pick-up mechanism, involving mechanistic steps that are generally barrierless. The results demonstrate that full ethene dehydrogenation is most favorable for intermediate-sized clusters, an observation supported for small clusters up to Nb_6 by the theoretical computations of reaction Gibbs energy changes. Computations support the proposal that the dehydrogenation mechanism involves production of H_2 as a product, and that the overall dehydrogenation becomes more favorable as the clusters become larger, due to weakening of the C−H bonds in the $Nb_nC_2H_2$ intermediate, and the associated thermodynamic advantage that this weakening imparts to the overall reaction Gibbs energy change. The primary product distribution observed supports the conclusion that the overall reaction to form fully dehydrogenated Nb_nC_2 species is barrierless, beyond the endergonicity of the process itself, where present.

Acknowledgment. This work was supported by the NSERC Discovery Grants program, the DGAPA (#IN124602), and the CONACYT-NSF (E120.1778/2001). The authors acknowledge Sara Jiménez Cortés and María Teresa Vázquez for technical support and DGSCA/UNAM (México) for providing computer time. A.G.-G. would like to thank the CONACYT for scholarship support. M.G.K.T. acknowledges the NSERC for scholarship support under the PGS program.

References and Notes

(1) Knickelbein, M. B. *Annu. Rev. Phys. Chem.* **1999**, *50*, 79.
(2) Kumar, V.; Kawazoe, Y. *Phys. Rev. B* **2002**, *65*, 125403.
(3) Goodwin, L.; Salahub, D. R. *Phys. Rev. A* **1993**, *47*, R774.
(4) Grönbeck, H.; Rosen, A. *Phys. Rev. B* **1996**, *54*, 1549.
(5) Grönbeck, H.; Rosen, A.; Andreoni, W. *Phys. Rev. A* **1998**, *58*, 4630.
(6) Roszak, S.; Majumdara, D.; Balasubramaniana, K. *J. Phys. Chem. A* **1999**, *103*, 5801.
(7) Jiao, C. Q.; Freiser, B. S. *J. Phys. Chem.* **1995**, *99*, 10723.
(8) Jiao, C. Q.; Ranatunga, D. R. A.; Freiser, B. S. *J. Phys. Chem.* **1996**, *100*, 4755.
(9) Berg, C.; Schindler, T.; Niedner-Schatteburg, G.; Bondybey, V. E. *J. Chem. Phys.* **1995**, *102*, 4870.
(10) Elkind, J. L.; Weiss, F. D.; Alford, J. M.; Laaksonen, R. T.; Smalley, R. E. *J. Chem. Phys.* **1988**, *88*, 5215.
(11) Morse, M. D.; Geusic, M. E.; Heath, J. R.; Smalley, R. E. *J. Chem. Phys.* **1985**, *583*, 2293.
(12) Zakin, M. R.; Brickman, R. O.; Cox, D. M.; Kaldor, A. *J. Chem. Phys.* **1988**, *88*, 3555.
(13) Lafleur, R. D.; Parnis, J. M.; Rayner, D. M. *J. Chem. Phys.* **1996**, *105*, 3551.
(14) Bérces, A.; Hackett, P. A.; Lian, L.; Mitchell, S. A.; Rayner, D. M. *J. Chem. Phys.* **1998**, *108*, 5476.
(15) Zakin, M. R.; Cox, D. M.; Kaldor, A. **1987**, *91*, 5224.
(16) Zakin, M. R.; Brickman, R. O.; Cox, D. M.; Kaldor, A. *J. Chem. Phys.* **1988**, *88*, 5943.
(17) St. Pierre, R. J.; Chronister, E. L.; El-Sayed, M. A. **1987**, *91*, 5228.
(18) Berg, C.; Schindler, T.; Lammers, A.; Niedner-Schatteburg, G.; Bondybey, V. E. *J. Chem. Phys.* **1995**, *99*, 15497.
(19) Ritter, D.; Carroll, J. J.; Weisshaar, J. C. **1992**, *96*, 10636.
(20) Carroll, J. J.; Haug, K. L.; Weisshaar, J. C.; Blomberg, M. R.; Siegbahn, P. E. M.; Svensson, M. *J. Phys. Chem.* **1995**, *99*, 13955.
(21) Carroll, J. J.; Haug, K. L.; Weisshaar, J. C. *J. Am. Chem. Soc.* **1993**, *115*, 6962.
(22) Blomberg, M. R.; Siegbahn, P. E. M.; Svensson, M. *J. Phys. Chem.* **1992**, *96*, 9794.
(23) Carroll, J. J.; Weisshaar, J. C. *J. Phys. Chem.* **1996**, *100*, 12355.

(24) Wen, Y.; Porembski, M.; Ferrett, T. A.; Weisshaar, J. C. *J. Phys. Chem. A* **1998**, *102*, 8362.

(25) Porembski, M.; Weisshaar, J. C. *J. Phys. Chem. A* **2000**, *104*, 1524.

(26) Jiao, C. Q.; Freiser, B. S. *J. Phys. Chem.* **1995**, *99*, 3969.

(27) Berg, C.; Schindler, T.; Kantlehner, M.; Niedner-Schatteburg, G.; Bondybey, V. E. *Chem. Phys.* **2000,** *262*, 143.

(28) Pedersen, D. B.; Parnis, J. M.; Lafleur, R. D.; Rayner, D. M. *J. Phys. Chem. A* **2004**, *108*, 2682.

(29) On-axis mass detection was employed for product mass analysis and the sequential kinetics analysis due to higher signal-to-noise ratio performance in this mode. Metal cluster removal rate analysis was done with data obtained from off-axis mass detection. No significant difference in the data obtained with the two configurations of detection used was noted, with the exception of improved resolution with off-axis detection at the expense of signal-to-noise which was somewhat worse.

(30) Pedersen, D. B.; Parnis, J. M.; Rayner, D. M. *J. Chem. Phys.* **1998**, *109*, 551.

(31) Mitchell, S. A.; Lian, L.; Rayner, D. M.; Hackett, P. A. *J. Chem. Phys.* **1995**, *103*, 5539.

(32) The difficulties are related with correlation and exchange effects of variable occupation of *n*d, $(n + 1)$s, and $(n + 1)$p valence orbitals, the lack of an unambiguous reference energy in approximate DFT, and relativistic effects. See, for example, Koch, W.; Holthausen, M. C. *A Chemist's Guide to Density Functional Theory*; Wiley-VCH: Weinheim, Federal Republic of Germany, 2001; pp 149−156.

(33) Gaussian 98, Revision A.11.4. Frisch, M. J.; Trucks, G. W.; Schlegel, H. B.; Scuseria, G. E.; Robb, M. A.; Cheeseman, J. R.; Zakrzewski, V. G.; Montgomery, J. A., Jr.; Stratmann, R. E.; Burant, J. C.; Dapprich, S., Millam, J. M.; Daniels, A. D.; Kudin, K. N.; Strain, M. C.; Farkas, O.; Tomasi, J.; Barone, V.; Cossi, M.; Cammi, R.; Mennucci, B.; Pomelli, C.; Adamo, C.; Clifford, S.; Ochterski, J.; Petersson, G. A.; Ayala, P. Y.; Cui, Q.; Morokuma, K.; Rega, N.; Salvador, P.; Dannenberg, J. J.; Malick, D. K.; Rabuck, A. D.; Raghavachari, K.; Foresman, J. B.; Cioslowski, J.; Ortiz, J. V.; Baboul, A. G.; Stefanov, B. B.; Liu, G.; Liashenko, A.; Piskorz, P.; Komaromi, I.; Gomperts, R.; Martin, R. L.; Fox, D. J.; Keith, T.; Al-Laham, M. A.; Peng, C. Y.; Nanayakkara, A.; Challacombe, M.; Gill, P. M. W.; Johnson, B.; Chen, W.; Wong, M. W.; Andres, J. L.; Gonzalez, C.; Head-Gordon, M.; Replogle, E. S.; Pople, J. A. Gaussian, Inc.: Pittsburgh, PA, 2002.

(34) Becke, A. D. *J. Chem. Phys.* **1993**, *98*, 5648. Stephens, P. J.; Devlin, J. F.; Chabalowski, C. F.; Frisch, M. J. *J. Phys. Chem.* **1994**, *98*, 11623.

(35) Hay, P. J.; Wadt, W. R. *J. Chem. Phys.* **1985**, *82*, 299.

(36) Hay, P. J.; Wadt, W. R. *J. Chem. Phys.* **1985**, *82*, 270.

(37) (a) Krishnan, R.; Binkley, J. S.; Seeger, R.; Pople, J. A. *J. Chem. Phys.* **1980**, *72*, 650. (b) Clark, T.; Chandrasekhar, J.; Spitznagel, G. W.; Schleyer, P. v. R. *J. Comput. Chem.* **1983**, *4*, 294. (c) Frisch, M. J.; Pople, J. A.; Binkley, J. S. *J. Chem. Phys.* **1984**, *80*, 3265. (d) McLean, A. D.; Chandler, G. S. *J. Chem. Phys.* **1980**, *72*, 5639.

(38) Müller, N.; Falk, A. Ball & Stick 3.7.6, molecular graphics software for MacOS, Johannes Kepler University: Linz, Austria, 2000; MOLEKEL 4.0 P. Flükiger, P.; Lüthi, H. P.; Portmann, S.; Weber, J. Swiss Center for Scientific Computing: Manno, Switzerland, 2000.

(39) τ is determined directly using the delay time between the cluster generation pulse and the detection pulse. The latter is multiplied by the fraction of the total flow reactor length over which the clusters are exposed to the reagent, to obtain τ.

(40) See for example: Steinfeld, J. I.; Francisco, J. S.; Hase, W. L. *Chemical Kinetics and Dynamics*, 2nd ed. Prentice-Hall: Englewood Cliffs, NJ, 1999; p 29.

(41) Knickelbein, M. B.; Yang, S. *J. Chem. Phys.* **1990**, *93*, 5760.

(42) Calculated C−H bond lengths (Å units) are 1.087 (NbC_2H_2), 1.090 ($Nb_2C_2H_2$), 1.091 ($Nb_3C_2H_2$), 1.095 ($Nb_4C_2H_2$), 1.097 ($Nb_5C_2H_2$), and 1.106 ($Nb_6C_2H_2$).

(43) Siegbahn, P. E. M.; Blomberg, M. R.; Svensson, M. *J. Am. Chem. Soc.* **1993**, *115*, 1952.

(44) Schnabel, P.; Weil, K. G.; Irion, M. P. *Angew. Chem., Int. Ed. Engl.* **1992**, *31*, 636.

(45) Berg, C.; Kaiser, S.; Schindler, T.; Kronseder, C.; Niedner-Schatteburg, G.; Bondybey, V. E. *Chem. Phys. Lett.* **1994**, *231*, 139.

(46) Note that the estimated error in total calculated Gibbs energy is ± 20 kJ mol^{-1}.

(47) Although we feel confident that we have established the global minima for these systems, we recognize that, were the global minima structures shown to have a significantly different structure, the trend in extent of dehydrogenation and its interpretation would need to be revisited.

(48) Data obtained from: *CRC Handbook of Chemistry and Physics*, 70th ed.; Weast, R. C.,Editor in Chief; CRC Press: Boca Raton FL, 1989−1990.